Research Article | Vol. 26, No. 16 | 6 Aug 2018 | OPTICS EXPRESS 20270
Optics EXPRESS

# Weak-scattering static diffuser by fast pumping dispersed-nanoparticles in a long distance using microfluidic flows for efficient laser speckle reduction

ZHAOMIN TONG,[1,2,*] WENZHI CHENG,[1,2] SUOTANG JIA,[1,2] AND XUYUAN CHEN[1,2,3]

[1]State Key Laboratory of Quantum Optics and Quantum Optics Devices, Institute of Laser Spectroscopy, Shanxi University, Taiyuan, Shanxi 030006, China
[2]Collaborative Innovation Center of Extreme Optics, Shanxi University, Taiyuan, Shanxi 030006, China
[3]Faculty of Technology, Natural Sciences and Maritime Sciences, Department of Microsystems, University of Southeast Norway, Borre N-3184, Norway
[*]zhaomin.tong@sxu.edu.cn

**Abstract:** Changing diffusers are most commonly used for laser speckle reduction. Here, a weak-scattering static diffuser (WSSD) is proposed and demonstrated by fast pumping poly(methyl methacrylate) nanoparticles in a long distance using microfluidic flow. Experimental results show that this proof-of-concept device can effectively reduce speckle, where the lowest speckle contrast ratio is 0.04. Comparing with vibrating/rotating diffusers driven by mechanical motors for speckle reduction, the WSSD is static. Moreover, the WSSD can suppress speckle with weaker light scatterings (scattering angle equals to 5.8° at the lowest speckle contrast ratio value), making it superior to vibrating/rotating diffusers driven by micro actuators. Because of these promising advantages, the WSSD has prospects of wide range of applications, such as in laser projection displays.



## 1. Introduction

The coherence property of electromagnetic waves, such as the waves produced by lasers, causes interference when they are scattered from a rough object, which is known as speckle [1]. Speckle is useful tool to measure displacement, deformation, surface roughness, etc [2–4]. However, in the applications of lasers in optical coherence tomography, holography, projection displays, etc., the bright and dark speckle grains induce noise and degrade image quality; therefore, speckle must be suppressed [5–7]. Among various kinds of laser speckle reduction techniques such as using random lasers [8], wavelength diversity [9], polarization diversity [10], angle diversity [11–13], binary diffusers [14,15], and specially designed screens [16], fast changing diffusers are most commonly used because they are simple and effective, where different speckle images are generated and averaged out by a detector (for example, human eyes) during its integration period [1,17–20].

A fast changing diffuser is generally realized by using a mechanical motor to vibrate/rotate the diffuser [17,18]. The introduction of micro actuators, such as electroactive polymers and deformable micro-mirrors, to vibrate/rotate the diffuser makes the device more compact and less power consumed [19,20]. However, according to the relationship between the scattered wave correlation area $A_c$ and the diffuser surface phase shifts $\sigma_\Phi$ as follows:

$$A_c = \frac{\pi r_c^2 e^{-\sigma_\phi^2}}{1-e^{-\sigma_\phi^2}}\left[Ei\left(\sigma_\phi^2\right)-\varepsilon-\ln\left(\sigma_\phi^2\right)\right], \quad (1)$$

where $r_c$ is the radius at which the normalized diffuser surface correlation falls to 1/e, $Ei$ is the exponential integral, and $\varepsilon$ is the Euler's constant, $A_c$ is inversely proportional to $\sigma_\Phi$ [1]; thus,

#332694 https://doi.org/10.1364/OE.26.020270
Journal © 2018 Received 30 May 2018; revised 18 Jul 2018; accepted 19 Jul 2018; published 25 Jul 2018

Optics EXPRESS

a higher scattering diffuser (larger $\sigma_\Phi$) creates a smaller scattered wave correlation area $A_c$, and vice versa. For the constant changing diffuser traveling area $A$, $M = A/A_c$ numbers of independent speckle images can be produced and the speckle contrast ratio (CR, which is defined as the ratio between the standard deviation and the mean value of speckle intensity) can be reduced by $1/M^{1/2} = (A_c/A)^{1/2}$ [1]. This relationship indicates that the speckle contrast is inversely proportional to the diffuser scattering angle. Therefore, because the range of motion of the micro actuator is limited (from micrometers to millimeters), a high scattering diffuser must be introduced to sufficiently reduce speckle [19,20].

In this paper, a weak-scattering static diffuser (WSSD) driven by a micropump for laser speckle reduction is proposed and demonstrated. The WSSD is composed of microfluidic chips made of polydimethylsiloxane (PDMS), where dispersed poly(methyl methacrylate) (PMMA) nanoparticles are quickly driven inside the micro-channels in circulation by the piezoelectric micropump. Because the microfluidic chip filled with the PMMA nanoparticles works as the diffuser, and the modulation is realized by the micropump, whose motion is isolated from the diffuser, the WSSD is motionless or static. The influences of the micro-channel dimension, the driving voltage and frequency of the micropump, the mass fraction of PMMA nanoparticles in the dispersion and the charge-coupled device (CCD) camera exposure time on speckle reduction efficiency are investigated. Due to the long traveling distance (large traveling area) of the PMMA nanoparticles during the CCD camera exposure time, speckle is efficiently reduced. Meanwhile, this static diffuser has a weak-scattering property because of the low PMMA nanoparticle concentration and the short light scattering distance. Thus, the conflict between the speckle reduction efficiency and the diffuser scattering angle in micro actuator driving diffusers is avoided. By using this proof-of-concept device, a lowest speckle contrast value of 0.04 is demonstrated, where the laser beam transmitting through the WSSD is weak-scattered with a scattering angle at 5.8°. Because of these promising characteristics, the WSSD may be more suitable on speckle reduction conditions with special requirements in light etendue, noise control, etc., such as in laser projection displays.

## 2. Microfluidic chip fabrication and experimental setup

### *2.1 Microfluidic chip fabrication*

We start the WSSD fabrication from the realization of microfluidic chips made of PDMS using soft-lithography methods [21]. Figure 1(a) shows the fabrication process. SU-8 photoresists are spin-coated onto polished 3-inch silicon wafers, which are exposed and developed to form master molds. Then, 3 mm thick mixtures of liquid PDMS and crosslinking agent are poured into the molds and heated. Once the mixtures are hardened, the PDMS replicas are taken off from the SU-8 molds, and micro-channels are formed. Next, the PDMS replicas are punched to obtain 1 mm diameter circular holes as inputs and outputs. In order to realize speckle reduction in the entire WSSD area, two pieces of flexible PDMS replicas and a 1 mm thick double-sided polished 3-inch glass wafer are aligned and bonded together after plasma treatments. Here, the micro-channels in the PDMS replicas are arranged in a staggered manner as shown in Fig. 1(b); the glass wafer is in the middle, and the critical dimension for the alignment is 10 μm. Before the bonding process, a 3 mm × 2 mm rectangular through-hole is drilled via the double-sides polished glass wafer to connect the top and bottom PDMS replicas. Finally, the microfluidic chip dies are split using a wafer dicing process. Figure 1(c) shows the picture of a fabricated microfluidic chip.

Optics EXPRESS

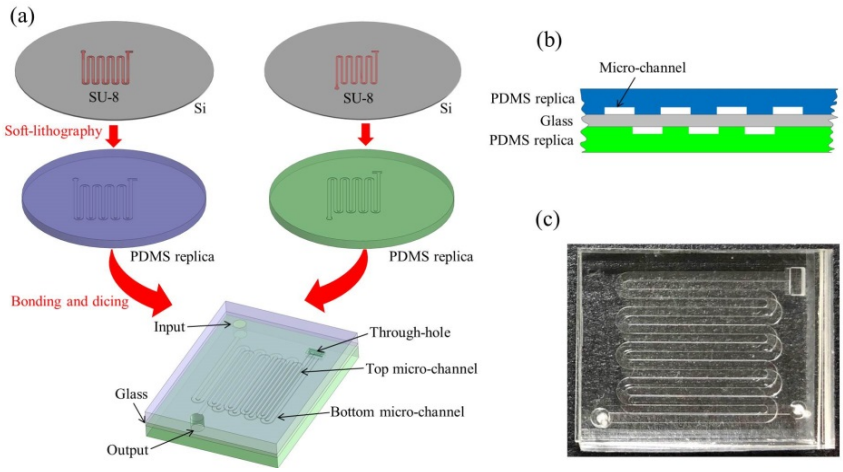


Fig. 1. (a) The fabrication process of the microfluidic chip. SU-8 is used to define patterns that are later transferred to the PDMS material using soft-lithography. Two pieces of PDMS replica and a double-sided polished glass wafer are bonded together to form the final device, where the PDMS replicas are connected via the through-hole on the glass wafer. (b) The micro-channels in the PDMS replicas are arranged in a staggered manner. (c) The picture of a fabricated microfluidic chip.

In order to increase the value of the diffuser surface phase shift $\sigma_\Phi$ in Eq. (1), the micro-channel heights $h$ shall be as large as possible. However, because the thickest spin-coated SU-8 film that is achievable in our lab is 300 μm, $h$ = 300 μm micro-channel height is used. The critical dimension during the alignment process (between the two pieces of PDMS replicas) is 10 μm, which indicates that less than or around 10 μm micro-channel widths are inappropriate. Considering the effect of refractive-index mismatch between the PDMS layer and the PMMA dispersion on speckle reduction that will be presented later, much larger than 10 μm micro-channel widths are preferred to study the speckle reduction efficiency with the WSSD. Therefore, hundreds of micrometers wide micro-channels are chosen as our first try. The microfluidic chips are fabricated within the same surface area dimension (10 mm × 10 mm square), where the working region of the microfluidic chips is an about 5 mm × 5mm square. Once the micro-channel widths are known, the micro-channel lengths can be determined according to the layout of the microfluidic chip. It is because these considerations on the microfabrication abilities and the possible application issues using the WSSD that four types of microfluidic chips with different micro-channel width $w$ and length $l$ are designed and fabricated, such as type1: $w_1$ = 200 μm and $l_1$ = 134.89 mm, type2: $w_2$ = 400 μm and $l_2$ = 92.98 mm, type3: $w_3$ = 600 μm and $l_3$ = 91.27 mm and type4: $w_4$ = 800 μm and $l_4$ = 70.25 mm.

### *2.2 Experimental setup*

The microfluidic chip is connected to the piezoelectric micropump (*Takasago Electric*, SDMP320) using stainless steel needles and Teflon tubes (inner diameter of 2.29 mm). PMMA nanoparticles (average particle size of 500 nm and refractive-index of 1.49-1.59) are dispersed in water under low mass fraction. The PMMA dispersion is driven in circulation inside the micro-channels by the piezoelectric micropump; thus, the WSSD with microfluidic flow driving nanoparticles is obtained. Figure 2 shows the experimental setup for laser speckle reduction measurements. A collimated temperature stabilized laser diode (*Thorlabs*, L520P50, linear polarized, central wavelength of 520 nm and optical power of 50 mW) is expanded as a 20 mm circular laser beam, followed by a rotating linear polarizer to adjust the optical power. A circular iris (aperture diameter of 5 mm) is used to define the effective laser beam illuminating on the WSSD, and the speckle image formed on the WSSD is recorded by

Optics EXPRESS

a CCD camera with the help of an imaging lens (focal length of 35 mm and F-number of 16), where the distance from the imaging lens to the WSSD is 45 mm.

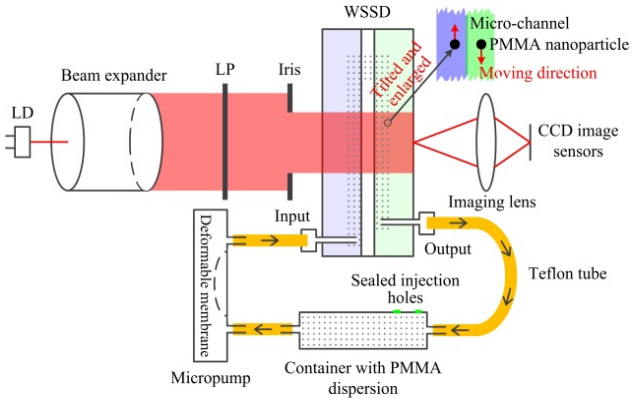


Fig. 2. The experimental setup to characterize the speckle reduction efficiency using the WSSD. The expanded laser beam illuminates the WSSD and generates speckles there. Speckle images are captured by the CCD camera. Because the PMMA dispersion is driven inside the micro-channel by the piezoelectric micropump, PMMA nanoparticles are fast traveling, which results in temporally changing speckle images during the CCD camera exposure time. Therefore, speckle reduction is achieved for the summer speckle image. LD: laser diode, LP: linear polarizer and CCD: charge-coupled device.

## 3. Results and discussion

For the WSSD, speckle reduction efficiency is determined by the number of independent speckle images that are generated and summed during the detector integration time. Therefore, when the micro-channel dimension or the driving voltage and frequency of the micropump are modified, the traveling velocity of PMMA nanoparticles, *i.e.*, the value of diffuser traveling area $A$, varies, which changes the speckle reduction efficiency. The influence of CCD camera exposure time on speckle reduction efficiency is straightforward, where longer CCD camera exposure time helps to obtain a lower speckle CR. The mass fraction of PMMA nanoparticles in the dispersion is the third factor influencing on speckle reduction efficiency, where the speckle reduction efficiency is determined both by the change of the traveling velocity of PMMA nanoparticles (because the viscosity of the PMMA dispersion is affected by the change of the mass fraction of PMMA nanoparticles) and the change of scattered wave correlation area $A_c$ (because the diffuser surface phase shifts $\sigma_\Phi$ is affected by the change of the mass fraction of PMMA nanoparticles).

### *3.1 Effect of the refractive-index mismatch on speckle reduction*

Figure 3 shows the speckle images captured by the CCD camera using the type2 micro-channel, where the mass fraction of PMMA nanoparticles in the dispersion is a constant value of 2.5%, and the CCD camera exposure time is set to 50 ms. The piezoelectric micropump is turned off (speckle image shown in Fig. 3(a)) and on (speckle image shown in Fig. 3(b)) to characterize the speckle reduction efficiency before and after driving the WSSD, respectively, where a signal generator with sinusoidal waveform of peak-to-peak voltage of 230 V and frequency of 50 Hz is used to drive the micropump. The speckle CRs are calculated as $C_{w\_b}$ = 1.08 for speckle image shown in Fig. 3(a) and $C_{w\_a}$ = 0.32 for speckle image shown in Fig. 3(b). These high speckle CRs are mainly caused by the non-uniform light distributions. As shown in Figs. 3(a) and 3(b), very obvious dark rectangular regions exist; thus, extra variations of speckle intensities are introduced, resulting in higher standard deviations and speckle CRs [1]. The presence of the dark rectangular regions is because of the mismatched refractive-indexes between the PDMS layer (refractive-index of 1.41) and the PMMA

Optics EXPRESS

dispersion (refractive-index of 1.33). More times of light reflection occurs in the dark rectangular regions, where the laser beam transmits through the PMMA dispersion twice; while the laser beam only transmits through the PMMA dispersion once for the other regions, resulting in less times of light reflection. It is because of the misalignment between the top and bottom PDMS replicas that the widths of the dark rectangular region are different. As shown in Fig. 1(b), two 20 μm wide overlapping regions are designed for a pair of staggered top and bottom micro-channels. However, after the alignment and bonding processes, the 10 μm critical dimension during the alignment process causes misalignment, and hence results in the unequal widths between two nearby dark rectangular regions.

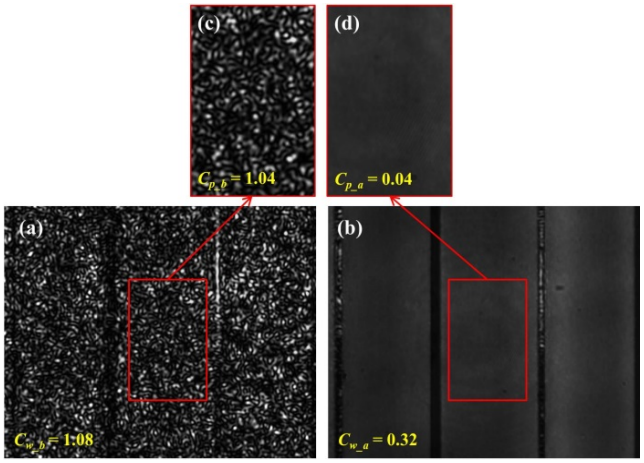


Fig. 3. (a) The speckle image using the WSSD by turning off the micropump. (b) The speckle image using the WSSD by turning on the micropump. (c) and (d) The speckle images after ignoring the dark rectangular regions shown in (a) and (b), respectively.

With the modification of the refractive-index of PMMA dispersion, such as by adding sodium chloride or calcium chloride in the dispersion [22], the refractive-index mismatch problem between the PDMS layer and the PMMA dispersion is expected to be solved, thus making the dark rectangular regions disappear [23]. However, the fluidic viscosity will increase accordingly, which decreases the traveling velocity of PMMA nanoparticles and consequentially leads to the sacrifice of speckle reduction efficiency. Another approach to preventing the presence of dark rectangular regions is to redesign the WSSD, such as by introducing one wide micro-channel and making it cover the entire laser transmission area. In this situation, the laser beam only transmits through the PMMA dispersion, thus avoiding the refractive-index mismatch and the dark rectangular regions. Here, the tradeoffs include the requirement of using a more powerful micropump because of the increased channel cross-section area and the decreased speckle reduction efficiency due to the reduced average microfluidic flow velocity that depends on the micro-channel dimensions. Because the fluid travels faster along the central region than the edge region in the micro-channel, the effect of the microfluidic flow velocity uniformity on speckle reduction efficiency is another topic that we shall study when using this approach.

If the dark rectangular regions shown in Figs. 3(a) and 3(b) are ignorable, the real effect of using fast traveling PMMA nanoparticles on speckle reduction can be characterized. Based on the current experimental results, this is equivalent to the condition when a uniform area that one micro-channel covers is selected. Figures 3(c) and 3(d) show the areas for speckle reduction efficiency characterization after ignoring the dark rectangular regions. The speckle CRs are calculated as $C_{p\_b}$ = 1.04 and $C_{p\_a}$ = 0.04 before and after driving the WSSD, respectively. Comparing with the speckle CRs obtained from Figs. 3(a) and 3(b), these values

Optics EXPRESS

are lower and correctly indicate the speckle reduction efficiency with the help of fast traveling PMMA nanoparticles.

### *3.2 Effect of the micro-channel dimension on speckle reduction*

The average microfluidic flow velocity $v$, *i.e.*, the traveling velocity of PMMA nanoparticles, across the channel cross-section for a rectangular micro-channel can be written as [24]

$$v = \frac{\Delta P h^2}{12\eta l}\left[1 - 0.63\frac{h}{w}\tanh(1.57\frac{w}{h})\right], \tag{2}$$

where $\Delta P$ is the pressure difference between the input $P_i$ and output $P_o$ of the micro-channel, $\eta$ is the fluid dynamic viscosity, and $h$, $w$ and $l$ are the height, width and length of the micro-channel, respectively. In Eq. (2), $\Delta P = P_i - P_o = F/wh$, where $F$ is the driving force of the micropump. After substituting the values of $h$, $w$ and $l$ into Eq. (2), we can find that $v$ equals to $0.26F/\eta$, $0.31F/\eta$, $0.24F/\eta$ and $0.25F/\eta$ for type1, type2, type3 and type4 micro-channels, respectively; thus, the type2 micro-channel can provide the lowest CR, and the type3 micro-channel can lead to the highest speckle CR.

Figure 4 shows the speckle CRs under different CCD camera exposure time for the four types of micro-channels after ignoring the dark rectangular regions presented in Figs. 3(a) and 3(b). Error bars are given by calculating the standard deviations of the speckle CRs when different areas similar to Fig. 3(c) and 3(d) are selected. The piezoelectric micropump works at a frequency of 50 Hz and a peak-to-peak voltage of 230 V, and the mass fraction of PMMA nanoparticles in the dispersion is a constant value of 2.5%; thus, the values of $F$ and $\eta$ are fixed.

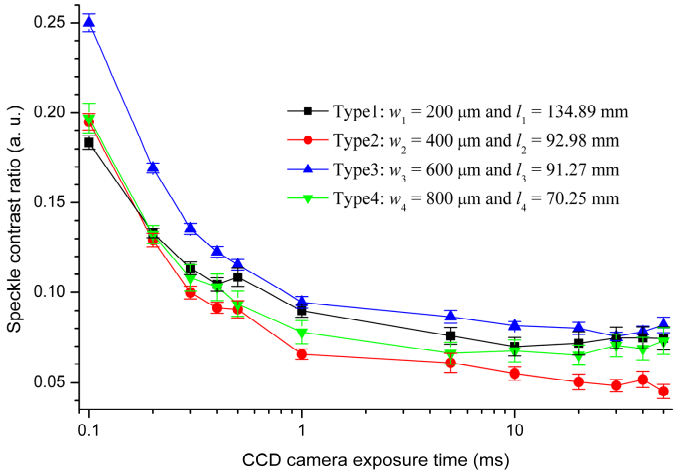


Fig. 4. The speckle CRs for the four types of micro-channels under different CCD camera exposure time. The dark rectangular regions as presented in Figs. 3(a) and 3(b) are neglected, and the driving force of the micropump $F$ and the fluid dynamic viscosity $\eta$ are fixed.

As shown in Fig. 4, type2 and type3 micro-channels, in general, can achieve the lowest and highest speckle CRs, respectively, and the speckle CRs for type1 and type4 micro-channels are almost equal. This is consistent with the calculated result based on Eq. (2), where the average microfluidic flow velocity, *i.e.*, the diffuser traveling area, is affected by the change of the micro-channel dimension. From Fig. 4, we can also find that the speckle CR decreases when the CCD camera exposure time become longer (because extra light intensity fluctuations for the recorded speckle images may be caused by the environmental influences such as the optical table vibration, the CCD camera noise, and the non-uniform illumination of the CCD chip, speckle CRs increase at several CCD camera exposure time). These trends

Optics EXPRESS

are reasonable because more independent speckle images are generated with the increase of the average microfluidic flow velocity or the CCD camera exposure time, thus decreasing the speckle CR after summing them together.

### *3.3 Effect of the driving voltage and frequency of the micropump on speckle reduction*

The *Takasago Electric* SDMP320 is a piezoelectric micropump with check valves [25]. This type of micropump can provide a wide linearly controllable pumping rate range and a high pumping pressure. A sinusoidal voltage waveform with peak-to-peak voltage from 60 V to 250 V and frequency from 10 Hz to 60 Hz can be used to modulate the pumping rate. Figure 5 shows the speckle CRs when the driving voltage (Fig. 5(a)) and the driving frequency (Fig. 5(b)) of the micropump are changed after ignoring the dark rectangular regions shown in Figs. 3(a) and 3(b). The type2 micro-channel is employed, and the other experimental conditions include 2.5% mass fraction of PMMA nanoparticles in the dispersion and 0.5 ms CCD camera exposure time.

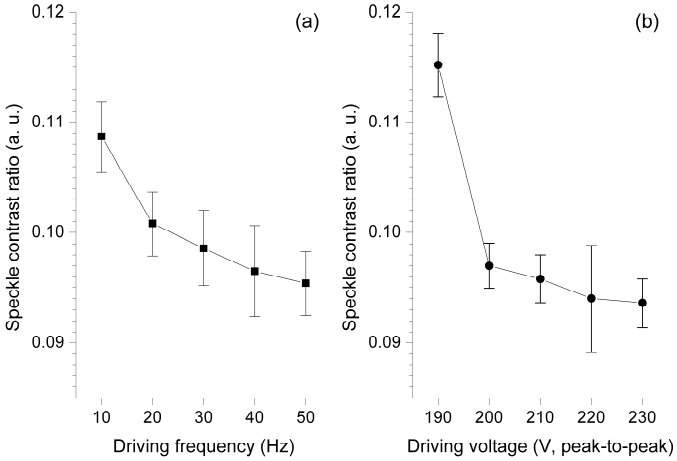


Fig. 5. (a) The speckle CRs when the driving frequency of the piezoelectric micropump is changed, where the driving voltage of the micropump is 230 V (peak-to-peak). (b) The speckle CRs when the driving voltage (peak-to-peak) of the piezoelectric micropump is changed, where the driving frequency of the micropump is 50 Hz.

As expected, the speckle CR decreases when the driving voltage or frequency of the micropump increases. With the increase of driving voltage or frequency, the higher pumping rate increases the traveling velocity of the PMMA nanoparticles and helps to reduce speckle.

### *3.4 Effect of the PMMA nanoparticle mass fraction on speckle reduction*

Figure 6 shows the speckle CRs with the change of the PMMA nanoparticle mass fraction after ignoring the dark rectangular regions shown in Figs. 3(a) and 3(b). We have used the type2 micro-channel. The piezoelectric micropump works at a frequency of 50 Hz and a peak-to-peak voltage of 230 V, and the CCD camera exposure time is 0.5 ms. From Fig. 6, we can find that the speckle CR decreases firstly when the PMMA nanoparticle mass fraction is increased from 1% to 2.5%; while the speckle effect becomes worse when the PMMA nanoparticle mass fraction grows from 2.5% to 3%.

Optics EXPRESS

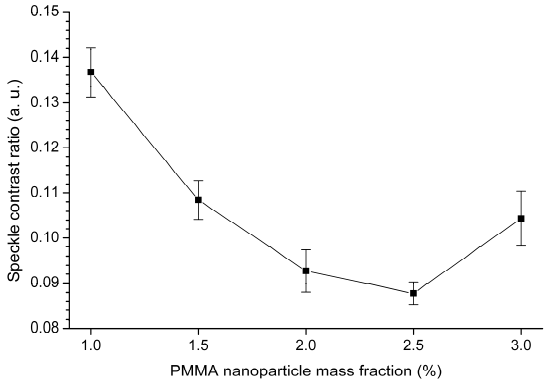


Fig. 6. The speckle CRs when the mass fraction of PMMA nanoparticles in the dispersion is changed from 1% to 3%. The driving voltage and frequency of the micropump and the CCD camera exposure time are fixed.

The mass fraction change of the PMMA nanoparticles in the dispersion has two effects on speckle reduction. First, it results in a viscosity change of the PMMA dispersion. The relative viscosity of a non-aggregating colloidal suspension and the particle volume fraction $\varphi$ (typically less than 4%) fulfill the following relationship

$$\eta_r = \frac{1}{(1-\varphi)^{2.5}}, \tag{3}$$

where $\eta_r$ is the relative viscosity defined as the ratio between the colloidal suspension $\eta$ and the base fluid $\eta_b$ [26]. The density of PMMA nanoparticle (1.05-1.2 g/mL) is close to that of water, so Eq. (3) is correct for the mass fraction of PMMA nanoparticles in the dispersion. According to Eq. (3), the viscosity of the PMMA dispersion increases non-linearly with the increase of PMMA mass fraction. Therefore, the average microfluidic flow velocity increases non-linearly after substituting Eq. (3) into Eq. (2). Second, the correlation area $A_c$ of the WSSD is affected by the change of the mass fraction of PMMA nanoparticles in the dispersion based on Eq. (1), where the laser correlation area $A_c$ of the WSSD decreases when the mass fraction of PMMA nanoparticles in the dispersion, *i.e.*, the diffuser surface phase shifts $\sigma_\Phi$, increases. Thus, more independent speckle images are generated and summed together during the CCD camera exposure time with the mass fraction increase of PMMA nanoparticles in the dispersion, and speckle CR becomes lower.

According to the above analysis, we can conclude that the changes in the PMMA dispersion viscosity and the scattered wave correlation area of the WSSD with the mass fraction of PMMA nanoparticles in the dispersion are opposite. Consequently, the speckle CR initially decreases and then increases for the mass fraction of PMMA nanoparticles in the dispersion changing from 1% to 2.5% (mainly determined by the change of the correlation area of the WSSD) and from 2.5% to 3% (mainly determined by the change of the viscosity of PMMA dispersion), respectively.

### *3.5 Optical power loss, scattering property, lifetime and comparison with changing diffusers driven by mechanical motors*

Interface reflections and PMMA nanoparticle backscatterings cause significant optical power loss for the current proof-of-concept WSSD. With the help of an integrating sphere optical power meter (*Thorlabs*, S142C), the optical powers before and after introducing the WSSD which produces the speckle images shown in Fig. 3 are characterized, where about 45% optical power is lost after using the WSSD. In order to suppress the optical power loss, a reflective-type WSSD with anti-reflective coatings is preferred for fabrication in the future.

Optics EXPRESS

The scattering property of the WSSD is characterized by comparing the laser beam widths before and after introducing the WSSD. In general, the scattering angle of a diffuser can be measured by a goniometer setup, where a small detector is scanned over a hemispherical surface centered after the diffuser to record the angular light intensity distribution [27]. Here, because the WSSD scattering angle is small, we have used a CCD camera beam profiler (*Thorlabs*, BC106N-VIS) to directly measure the angular light intensity distribution by placing it closely after the WSSD in Fig. 2. The distance from the micro-channels to the CCD sensors is 18 mm. In order to confine the scattered laser beam within the CCD camera beam profiler sensor area (8.77 mm × 6.6 mm), the aperture of the circular iris is adjusted down to 2.78 mm. After driving the WSSD, the scattered light intensity distribution is measured, and hence the $1/e^2$ laser beam width is obtained as 6.44 mm. Therefore, the scattering angle of the WSSD in this circumstance can be calculated as $180 \times \tan^{-1}[(6.44\text{-}2.78)/(2 \times 18)]/\pi = 5.8°$.

Micro-channels made of PDMS and micropumps normally have long lifetimes. The lifetime of the WSSD is mainly determined by the stability of the PMMA dispersion. Agglomeration and sedimentation of nanoparticles may occur after long-term use of the PMMA dispersion (for example, longer than twelve months). Therefore, in order to extend the lifetime of the device, regular replacements of the PMMA dispersion are recommended when using the device in practice. The deposition of PMMA nanoparticles on the walls of the micro-channels is observed during our experiments. The presence of this thin deposited layer makes light more scattering, but it has no bad effects on speckle reduction. In fact, if the deposited layer becomes thick, it will make the WSSD work as double diffusers where one is moving (the fast traveling PMMA nanoparticles) and the other is stationary (thin deposited layer of PMMA nanoparticles on the micro-channel walls); it is well known that the former can reduce speckle more efficiently than the latter. Because along with the deposition of the PMMA nanoparticles, microfluidic flow also etches the deposited layer; thus, the thickness of this deposited layer does not increase under a constant operation of the WSSD, and we have ignored this effect when analyzing the experimental results.

In order to compare the speckle reduction efficiency with changing diffusers driven by mechanical motors under the same experimental setup shown in Fig. 2, a commercialized ground glass diffuser (*Thorlabs*, DG100X100-120) with a diffusing angle of 15° (data provided by *Thorlabs*) and a linear motor (*Thorlabs*, LNR50K1) have been used. Figure 7 shows the speckle CRs for different linear motor traveling velocity, where 0.5 ms and 50 ms CCD camera exposure time have been used in Figs. 7(a) and 7(b), respectively.

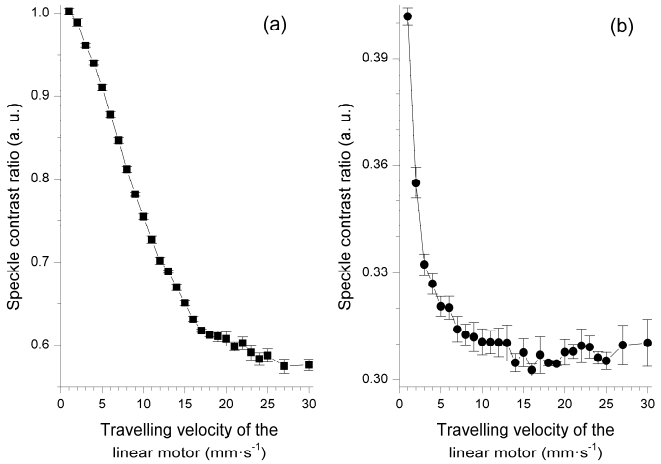


Fig. 7. The speckle CRs for different linear motor traveling velocity under the same experimental setup shown in Fig. 2, where (a) 0.5 ms and (b) 50 ms CCD camera exposure time have been used.

Optics EXPRESS

According to Fig. (7), we can find that the speckle CRs are about 0.58 and 0.3 at the maximum traveling velocity of the linear motor of 30 mm·s$^{-1}$ during 0.5 ms and 50 ms CCD camera exposure time, respectively; these values are about 0.09 and 0.04 when using the WSSD with the type2 micro-channel during the same CCD camera exposure time. Because the speckle reduction mechanism is the average of temporally generated different speckle images, thus, in order to bring the speckle CRs down to the same levels as the WSSD, the traveling velocity of the ground glass diffuser should to be about forty-nine (the mean value of $(0.58/0.09)^2 = 42$ and $(0.3/0.04)^2 = 56$) times greater than the current value, which equals to 1470 mm·s$^{-1}$.

If a rotating diffuser with a diffusing angle of 15° is employed in laser projection displays, and if the speckle image is perceived by human eyes with 50 ms integration time [28], in order to achieve the equivalent speckle reduction efficiency as the WSSD, the traveling distance of the diffuser should be $1470 \times 0.05 = 73.5$ mm. Therefore, the diameter of the rotating diffuser should be $73.5/\pi = 23.4$ mm when the edge of the rotating diffuser is used, and the rotation speed of the motor should be $1470 \times 60/73.5 = 1200$ rpm.

## 4. Conclusions

In conclusion, we have designed and fabricated a proof-of-concept WSSD to replace the generally used vibrating/rotating diffusers driven by mechanical motors or micro-actuators for laser speckle reduction. The aspects that affect the speckle reduction efficiency using the WSSD were investigated. We found that the faster PMMA nanoparticle traveling velocity, the longer CCD camera exposure time and the smaller scattered wave correlation area help to achieve lower speckle CRs. The weak-scattering and motionless characteristics of the WSSD make it have prospects of wide range of applications, such as in laser projection displays.

## Funding

National Key Research and Development Program of China (2016YFB0401903); Key Research and Development Program of Shanxi Province for International Cooperation (201703D421015); Changjiang Scholars and Innovative Research Team in University of Ministry of Education of China (IRT13076); State Key Program of National Natural Science of China (11434007).

## References

1. J. W. Goodman, “Dependence of speckle on scatterer microstructure” in *Speckle phenomena in optics: theory and applications* (Roberts and Company Publishers, 2006), pp. 84–105.
2. D. J. Chen, F. P. Chiang, Y. S. Tan, and H. S. Don, “Digital speckle-displacement measurement using a complex spectrum method,” Appl. Opt. **32**(11), 1839–1849 (1993).
3. A. J. Moore, D. P. Hand, J. S. Barton, and J. D. Jones, “Transient deformation measurement with electronic speckle pattern interferometry and a high-speed camera,” Appl. Opt. **38**(7), 1159–1162 (1999).
4. R. A. Sprague, “Surface roughness measurement using white light speckle,” Appl. Opt. **11**(12), 2811–2816 (1972).
5. B. Karamata, K. Hassler, M. Laubscher, and T. Lasser, “Speckle statistics in optical coherence tomography,” J. Opt. Soc. Am. A **22**(4), 593–596 (2005).
6. H. Lin and P. Yu, “Speckle mechanism in holographic optical imaging,” Opt. Express **15**(25), 16322–16327 (2007).
7. K. V. Chellappan, E. Erden, and H. Urey, “Laser-based displays: a review,” Appl. Opt. **49**(25), F79–F98 (2010).
8. B. Redding, M. A. Choma, and H. Cao, “Speckle-free laser imaging using random laser illumination,” Nat. Photonics **6**(6), 355–359 (2012).
9. J. Kinoshita, H. Aizawa, A. Takamori, K. Yamamoto, H. Murata, and K. Tojo, “Angular dependence of screen speckle and fiber speckle of coupled output of nine high-power blue laser diodes through a multi-mode fiber,” Opt. Rev. **23**(1), 121–132 (2016).
10. Z. Tong and X. Chen, “Speckle contrast for superposed speckle patterns created by rotating the orientation of laser polarization,” J. Opt. Soc. Am. A **29**(10), 2074–2079 (2012).
11. M. N. Akram, Z. Tong, G. Ouyang, X. Chen, and V. Kartashov, “Laser speckle reduction due to spatial and angular diversity introduced by fast scanning micromirror,” Appl. Opt. **49**(17), 3297–3304 (2010).
12. T. T. Tran, Ø. Svensen, X. Chen, and M. N. Akram, “Speckle reduction in laser projection displays through angle and wavelength diversity,” Appl. Opt. **55**(6), 1267–1274 (2016).

Optics EXPRESS


13. Z. Tong, W. Shen, S. Song, W. Cheng, Z. Cai, Y. Ma, L. Wei, W. Ma, L. Xiao, S. Jia, and X. Chen, "Combination of micro-scanning mirrors and multi-mode fibers for speckle reduction in high lumen laser projector applications," Opt. Express **25**(4), 3795–3804 (2017).
14. J. I. Trisnadi, "Hadamard speckle contrast reduction," Opt. Lett. **29**(1), 11–13 (2004).
15. J. Lee, T. Kim, B. Yim, J. Bu, and Y. Kim, "Speckle reduction in laser picoprojector by combining optical phase matrix with twin green lasers and oscillating MEMS mirror for coherence suppression," Jpn. J. Appl. Phys. **55**(8S3), 08RF03 (2016).
16. J. Pauwels and G. Verschaffelt, "Speckle reduction in laser projection using microlens-array screens," Opt. Express **25**(4), 3180–3195 (2017).
17. S. Kubota and J. W. Goodman, "Very efficient speckle contrast reduction realized by moving diffuser device," Appl. Opt. **49**(23), 4385–4391 (2010).
18. J. Pan and C. Shih, "Speckle noise reduction in the laser mini-projector by vibrating diffuser," J. Opt. **19**(4), 045606 (2017).
19. H. Farrokhi, T. M. Rohith, J. Boonruangkan, S. Han, H. Kim, S. W. Kim, and Y. J. Kim, "High-brightness laser imaging with tunable speckle reduction enabled by electroactive micro-optic diffusers," Sci. Rep. **7**(1), 15318 (2017).
20. H. A. Chen, J. W. Pan, and Z. P. Yang, "Speckle reduction using deformable mirrors with diffusers in a laser pico-projector," Opt. Express **25**(15), 18140–18151 (2017).
21. P. Kim, K. Kwon, M. Park, S. Lee, S. Kim, and K. Suh, "Soft lithography for microfluidics: a review," Biochip J. **2**(1), 1–11 (2008).
22. C. Tan and Y. Huang, "Dependence of refractive index on concentration and temperature in electrolyte solution, polar solution, nonpolar solution, and protein solution," J. Chem. Eng. Data **60**(10), 2827–2833 (2015).
23. A. Uçar and D. Velev, "Microfluidic elastomer composites with switchable vis-IR transmittance," Soft Matter **8**(44), 11232–11235 (2012).
24. M. Bahrami, M. Yovanovich, and J. Culham, "Pressure drop of fully-developed, laminar flow in microchannels of arbitrary cross-section," J. Fluid Eng. **128**, 1036–1044 (2006).
25. G. Feng and E. Kim, "Micropump based on PZT unimorph and one-way parylene valves," J. Micromech. Microeng. **14**(4), 429–435 (2004).
26. S. Halelfadl, P. Estelle, B. Aladag, N. Doner, and T. Mare, "Viscosity of carbon nanotubes water-based nanofluids: Influence of concentration and temperature," Int. J. Therm. Sci. **71**, 111–117 (2013).
27. D. Roßkamp, F. Truffer, S. Bolay, and M. Geiser, "Forward scattering measurement device with a high angular resolution," Opt. Express **15**(5), 2683–2690 (2007).
28. S. Roelandt, Y. Meuret, G. Craggs, G. Verschaffelt, P. Janssens, and H. Thienpont, "Standardized speckle measurement method matched to human speckle perception in laser projection systems," Opt. Express **20**(8), 8770–8783 (2012).